Hyoungsoon Lee[1,2]
School of Mechanical Engineering,
Chung-Ang University,
84, Heukseok-ro,
Dongjak-gu 06974, Seoul, South Korea
e-mail: leeh@cau.ac.kr

Tanmoy Maitra[2]
Mechanical Engineering,
University College London,
Gower St. Bloomsbury,
London WC1E 6BT, UK
e-mail: t.maitra@ucl.ac.uk

James Palko
Department of Mechanical Engineering,
University of California, Merced,
5200 N. Lake Rd,
Merced, CA 95343
e-mail: jpalko@ucmerced.edu

Daeyoung Kong
School of Mechanical Engineering,
Chung-Ang University,
84, Heukseok-ro,
Dongjak-gu 06974, Seoul, South Korea
e-mail: kongdy000@cau.ac.kr

Chi Zhang
Department of Mechanical Engineering,
Stanford University,
440 Escondido Mall,
Stanford, CA 94305
e-mail: chzhang@stanford.edu

Michael T. Barako[3]
Department of Mechanical Engineering,
Stanford University,
440 Escondido Mall,
Stanford, CA 94305
e-mail: mbarako@stanford.edu

Yoonjin Won
Department of Mechanical and Aerospace Engineering,
University of California, Irvine,
4200 Engineering Gateway,
Irvine, CA 92697
e-mail: won@uci.edu

Mehdi Asheghi
Department of Mechanical Engineering,
Stanford University,
440 Escondido Mall,
Stanford, CA 94305
e-mail: masheghi@stanford.edu

Kenneth E. Goodson
Department of Mechanical Engineering,
Stanford University,
440 Escondido Mall,
Stanford, CA 94305
e-mail: goodson@stanford.edu

Enhanced Heat Transfer Using Microporous Copper Inverse Opals

Enhanced boiling is one of the popular cooling schemes in thermal management due to its superior heat transfer characteristics. This study demonstrates the ability of copper inverse opal (CIO) porous structures to enhance pool boiling performance using a thin CIO film with a thickness of ∼10 μm and pore diameter of 5 μm. The microfabricated CIO film increases microscale surface roughness that in turn leads to more active nucleation sites thus improved boiling performance parameters such as heat transfer coefficient (HTC) and critical heat flux (CHF) compared to those of smooth Si surfaces. The experimental results for CIO film show a maximum CHF of 225 W/cm^2 (at 16.2 °C superheat) or about three times higher than that of smooth Si surface (80 W/cm^2 at 21.6 °C superheat). Optical images showing bubble formation on the microporous copper surface are captured to provide detailed information of bubble departure diameter and frequency.
[DOI: 10.1115/1.4040088]

[1]Corresponding author.
[2]The authors contributed equally to the paper.
[3]Present address: NG Next, Northrop Grumman Corporation, 1 Space Park, Redondo Beach, CA 90278.
Contributed by the Electronic and Photonic Packaging Division of ASME for publication in the JOURNAL OF ELECTRONIC PACKAGING. Manuscript received January 9, 2018; final manuscript received April 12, 2018; published online May 9, 2018. Assoc. Editor: Kaushik Mysore.

Introduction

The current performance of supercomputers, power devices, electric vehicles, and advanced military avionics is often limited by the ability to dissipate heat. An enhanced cooling of high heat flux applications performance of high heat flux electronic devices

[1–4]. The increase in total power dissipation requirements over small area has initiated significant interest in phase change cooling schemes, and the recent advancements in material development and nano/micro fabrication technologies have created tremendous possibilities for enhanced phase change heat transfer such as via structured surface, porous media, and three-dimensional manifold cooling configurations [5–17].

Micro/nanoscale surface modifications have been investigated by many researchers especially for thermal management solutions in high power density devices, since they allow remarkable increases in both heat transfer coefficient (HTC) and critical heat flux (CHF) [5–7,11–17]. Dhillon et al. [5] integrated nanotextured surfaces on Si micropillars and dissipated heat fluxes up to 211 W/cm^2. Chu et al. [6] used similar Si structured surfaces and dissipated 208 W/cm^2 from 2 cm × 2 cm test sample with water as a working fluid. Chen et al. [13] used nanowires on Si substrate and achieved CHF up to 226 W/cm^2 using water as a working fluid. Recently, Mori et al. and Jaikumar and Kandlikar reported very high CHF values of 306 W/cm^2 and 420 W/cm^2, respectively [14,15]. Mori et al. used a honeycomb porous plate on a nanoparticle-deposited surface while Jaikumar and Kandlikar used microchannel with sintered surface. However, there is still a lack of fundamental understanding of the influence of surface and bubble characteristics on the heat transfer performance, and there are limited reliable tools for accurate prediction of heat transfer characteristics.

Inverse opal structures are one of the porous matrices which have been widely used in various optical applications due to their superior tunable periodicities, diffractive and optical properties [18]. Metal inverse opal structure can be a promising material for microfluidic heat exchangers due to the high thermal conductivity with the relatively high permeability compared to other porous metals such as sintered cooper, woodpile scaffolds, or nanowire networks [18]. However, there has been relatively little research aimed at investigating thermal performance and heat transfer characteristics of inverse opal structures [16–18].

In this study, we fabricate copper inverse opals (CIO) to explore their boiling heat transfer characteristics. A highly instrumented pool boiling apparatus is used to measure accurate heat transfer coefficients and critical heat flux of the microporous copper inverse opal film. Flow visualization provides detailed bubble departure geometry and frequency in different heat flux ranges. The heat transfer performance of CIO is compared to a plain Si surface in boiling. This study provides useful information on the effect of microporous coatings on heat transfer characteristics in boiling.

Preparation of Copper Inverse Opals

Inverse opal structures are fabricated on the Si substrate by electrodeposition of copper around polystyrene (PS) spheres that served as sacrificial templates. The detailed fabrication process is described in Fig. 1. First, a cathode for electrodeposition, consisting of a 20 nm titanium adhesion layer under a 100 nm gold layer, is sputter coated (Oerlikon Leybold Univex 400 RF/DC) on a monocrystalline polished silicon wafer. A 4% weight/volume PS/water suspension is diluted 1:10 with de-ionized water, and ~60 μl of the diluted PS/water suspension is dispensed at once on the gold-coated silicon surface using a drop casting method (step (a) in Fig. 1) [19], and a circular silicone cutout with a diameter of ~1.5 cm is used to shape the flow after the dispensing droplet. The wafer is heated at ~50 °C on a hot plate while blowing air to evaporate the solvent (water) without coffee ring effect, as described in step (b) in Fig. 1. Thereafter, PS-coated silicon chips are heated in an oven at 103 °C for one hour to sinter PS spheres and form necks between the spheres, as depicted in step (c) in Fig. 1. Then, copper is electrodeposited galvanostatically into the PS template and aqueous 0.6 M $CuSO_4$ + 0.03 M H_2SO_4 electrolyte [20]. A single-channel potentiostat (Gamry Reference 600) is used in a three-electrode electrochemical cell consisting of the gold-coated silicon as a cathode, copper plate as an anode, and a Ag/AgCl (BaSi, Inc., West Lafayette, IN) reference electrode [20].

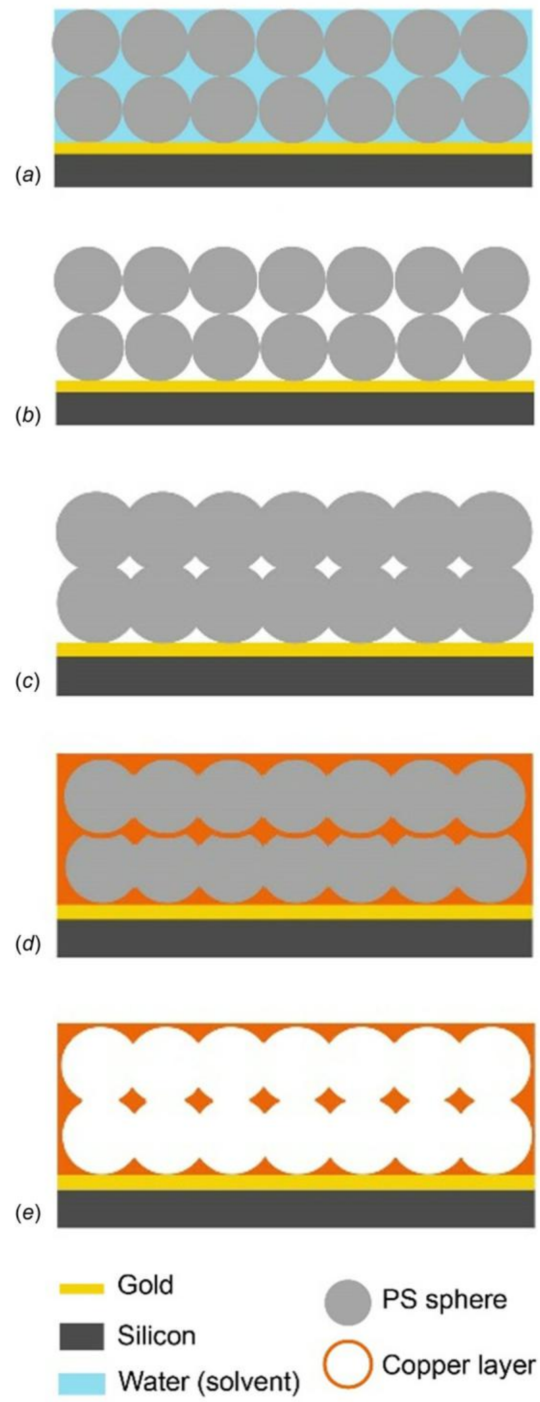

Fig. 1 Microporous copper fabrication process: (*a*) drop casting PS spheres on Au layer, (*b*) heating at 50 °C to evaporate water (solvent), (*c*) heating at 103 °C for one hour to sinter PS spheres, (*d*) electrodeposition of copper, and (*e*) dissolution of PS spheres in THF

The electrodeposition is performed at a fixed current density of 20 mA/cm^2 for 12 min to achieve ~10 μm copper layer thickness (step (d) in Fig. 1). Finally, PS spheres are dissolved in tetrahydrofuran (THF) for at least 24 h to reveal the porous copper structures (step (e) in Fig. 1). Colloidal suspensions of 5 μm spheres PS in water were purchased from Thermo Fisher Scientific. Tetrahydrofuran (anhydrous, > 99.9%), copper (II) sulfate (anhydrous,

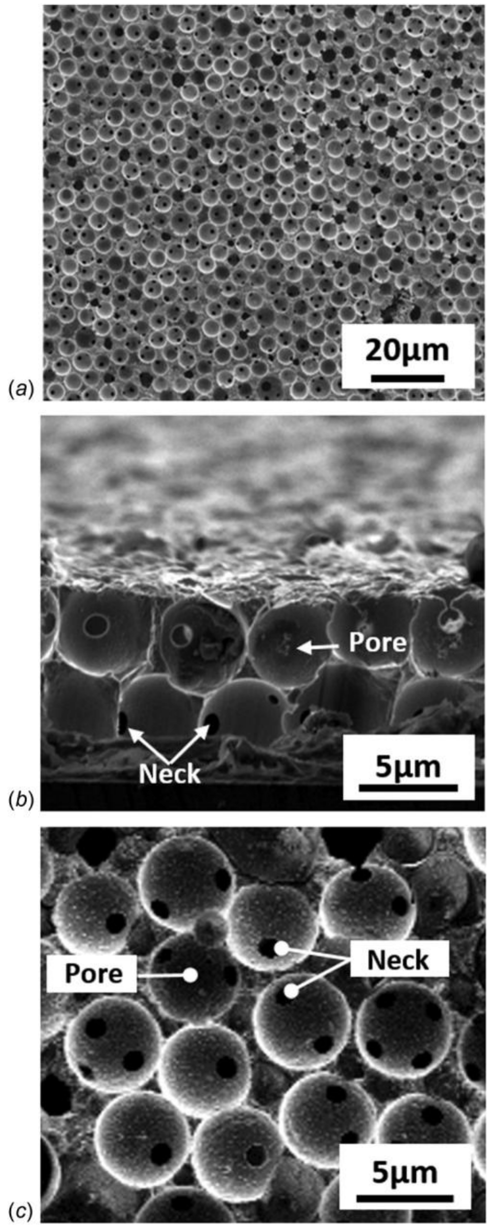

Fig. 2 Scanning electron microscopy graphs of microporous copper structures after dissolution of template (step (e) in Fig. 1): (*a*) top view, (*b*) cross-sectional view, and (*c*) pores and necks. CIO sample is fabricated using 5 μm sacrificial spheres.

powder, >99.9% trace metals basis), and sulfuric acid (~99.99%, density 1.840 g/ml) were purchased from Sigma Aldrich and used without further purification. Figure 2 shows scanning electron micrographs of a CIO structure which was used in the pool boiling tests. This sample was prepared using 5 μm PS spheres and 10 μm thick electrodeposition.

Experimental Apparatus

Heat transfer characteristics of CIO samples are measured using a customized pool boiling setup as shown in Fig. 3. The experimental setup consists of a transparent chamber which is made of four polycarbonate (Lexan) side walls for bubble visualization. DI water is used as a working fluid for the experiment, and it is degassed by vigorous boiling at ambient pressure ($T_{\mathrm{sat}} = 100\,^{\circ}\mathrm{C}$) for ~30 min on a hot plate before the experiment. Then, water is poured into a boiling chamber. Two immersion heaters and a coiled condenser are installed on the chamber for closed loop

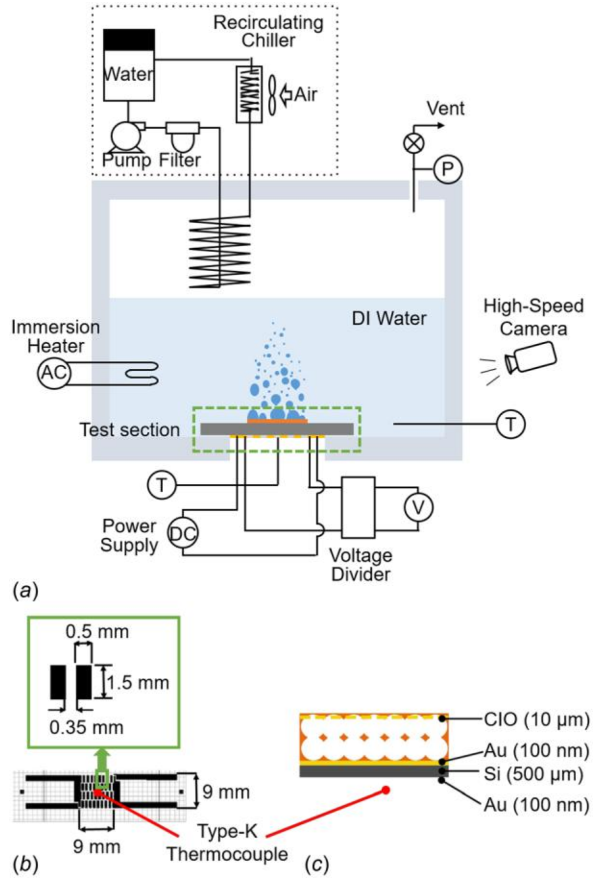

Fig. 3 Experimental apparatus (*a*) pool boiling apparatus, (*b*) thin film gold resistive mesh heater, and (*c*) cross-sectional view of test section (not scaled to size)

testing. The coiled condenser is connected to an external chiller (ThermoFlex 3500) to condense the evaporated working fluid into the liquid. The test sample is located on the bottom plate and all the electrical wiring is connected through a hole located at the center of the bottom plate. A thin film gold resistive heater with a heated area of $9 \times 9\,\mathrm{mm}^2$ is fabricated on the opposite side of the silicon substrate to supply heat for boiling experiments. A thickness of 100 nm-Au with a 10 nm-Ti adhesion layer is deposited by e-beam evaporation, and the metallic film is then patterned to square mesh shape using laser ablation (3 W diode pumped solid state laser with 355 nm, power of 20%, frequency of 120 kHz, and scanning speed of 2000 mm/s). This patterned mesh provides relatively uniform heater temperature over the heated area during boiling experiments due to current redistribution at the hot spot area. The exposed surface of the heater is insulated by a quarter inch silicone pad to minimize parasitic thermal losses during the test. Two regulated DC power supplies provide up to 1800 W electrical power to the heater. Total power input to the heater is measured using a customized voltage divider in parallel with the heater to avoid any electrical damage to the data acquisition system (USB-6251). The voltage divider consists of a 5 k$\Omega \pm 0.1$% resistor and a 45 k$\Omega \pm 0.1$% resistor in series providing a 10$\times$ reduction in voltage at the 5 kΩ sensing resistor. A low resistance shunt resistor of 0.05 $\Omega \pm 0.1$% is used to measure the current flowing through the heater. Voltage measurement accuracy in the data acquisition system is $\pm$0.02%, and overall uncertainty in CHF is $\pm$0.4%.

The heater temperature is measured using the change in resistance of the heater, which has been calibrated in an oven over a range of 25–120 °C. The resistance is obtained using a four-probe measurement technique. Two K-type thermocouples are also used

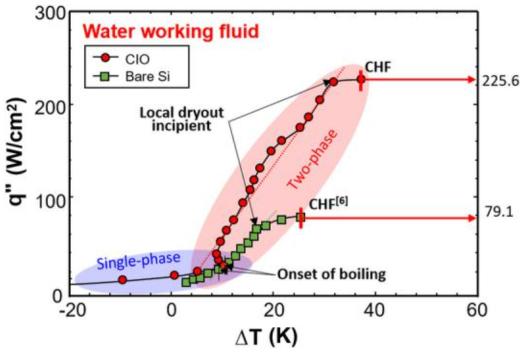

Fig. 4 Comparisons of boiling curves for the microporous copper structure with a pore diameter of 5 μm and plain Si surface [6]

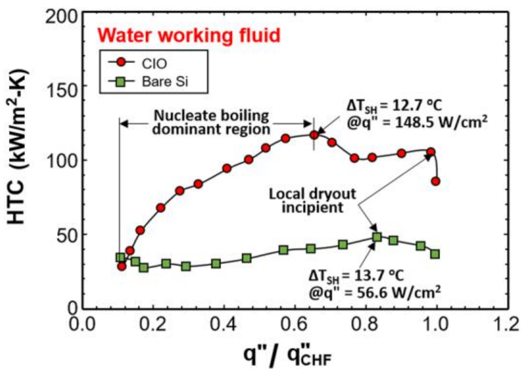

Fig. 5 Heat transfer coefficient versus normalized heat flux for the microporous copper structure with a pore diameter of 5 μm and plain Si surface

to measure the hot spot temperature of the heater and the working fluid temperature. The hot spot temperature is used to shutoff the power input when there is a sudden temperature rise corresponding to critical heat flux. Boiling images are obtained using a Phantom high-speed camera with two separate white light-emitting diode light sources. All images presented in this study are captured at 2 kHz.

Results and Discussions

The heat flux versus wall superheat of copper inverse opals in pool boiling is shown in Fig. 4. The wall superheat, ΔT_{SH}, is determined from a temperature difference between the averaged heated surface temperature, T_w, and the saturation temperature of the working fluid, T_{sat}. The results show significant enhancements in both CHF (Fig. 4) and heat transfer coefficient (Fig. 5) of the 5 μm CIO sample compared to those of a plain Si surface which were reported by Chu et al. [6]. The CIO sample shows a maximum CHF of 225.6 W/cm^2 showing a 3× enhancement of CHF compared to the plain surface (79.1 W/cm^2). We hypothesize that these superior heat transfer characteristics are mainly due to rapid water replenishment and significant enhanced heat transfer area provided by the CIO structure. For the same reasons, the effective heat transfer coefficient is much higher for the CIO sample as shown by the slope of the two-phase region in Fig. 4, which results in smaller wall superheat temperature at the corresponding heat flux over the entire nucleate boiling region compared to the plain Si surface. It should be noted that there is a slightly higher superheat temperature (ΔT_{SH}) at the onset of boiling (ONB) for the CIO compared to ΔT_{SH} of the plain Si. Also, a clear ONB is observed for the CIO, which is not observed for the plain Si. As reported by other researchers, no significant ONB for the plain Si is mainly caused by the inconsistencies in the inception of boiling for plain Si [21,22]. However, more detailed study is required to explore the effect of porous copper coating on ONB.

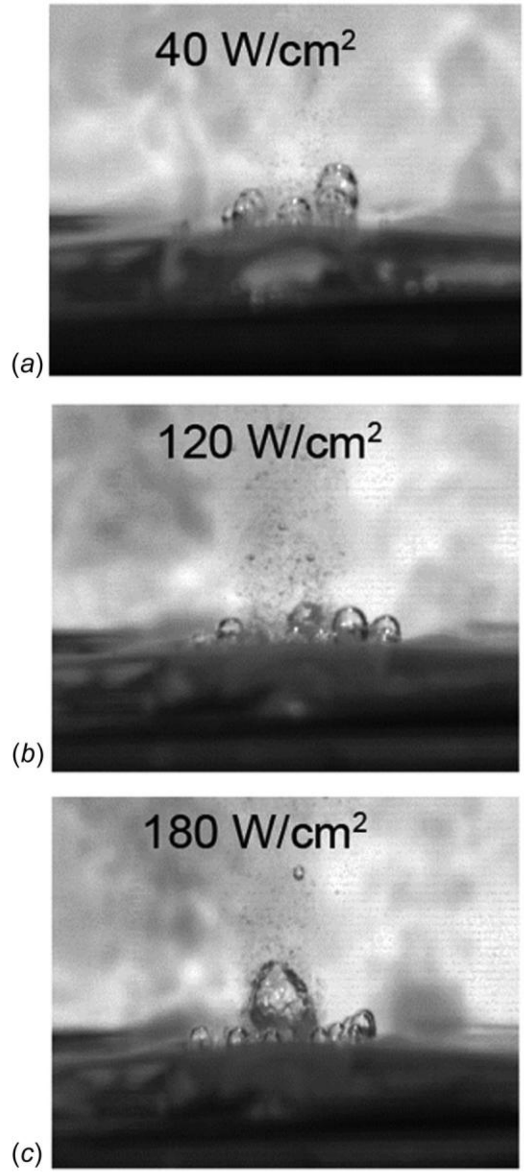

Fig. 6 Flow visualization of pool boiling on the microporous CIO structure with pore diameters of 5 μm at heat fluxes of (*a*) 18% (40 W/cm^2), (*b*) 53% (120 W/cm^2), and (*c*) 80% (180 W/cm^2) of CHF

Figure 5 shows the effective HTC versus the normalized heat flux, q''/q''_{CHF} for both the CIO and plain Si surface. The effective heat transfer coefficient is calculated from a ratio of heat flux based on the heated area and the temperature difference between top surface of the silicon substrate, T_{si}, and the saturation temperature of the working fluid, T_{sat}. A temperature drop due to conduction loss through the silicon substrate is considered to estimate T_{si}. HTC for the plain Si shows a range of 27.5–48.0 kW/m^2 K, which is similar but slightly higher compared to the values reported in Chen et al. [13]. The CIO sample shows a wide range of HTC 30–110 kW/m^2 K, which is more than a 2× improvements over the plain silicon. The larger surface area of the CIO provides lower thermal resistance, which results in lower temperature at the boiling surface. The superheat temperature ranging from 8.3 to 9.7 K for the CIO at $q''=$ 50 W/cm^2 is ~35% lower than plain Si at the corresponding heat flux.

Figure 6 shows optical images of bubbles on the CIO sample at three different heat fluxes of 18% (40 W/cm^2), 53% (120 W/cm^2), and 80% (180 W/cm^2) of CHF. As shown in this figure, there are two dominant bubble sizes observed during the test. Most of the bubbles departing from the center of the surface has smaller departure diameter of $D_b <\sim 1$ mm, and the bubble sizes are decreased right after departing from the surface due to the low bulk fluid temperature (i.e., less than T_{sat}). Also, there are large bubbles ($D_b = \sim$3–4 mm) observed at the boundary of the CIO. Since the Si surface has different surface characteristics compared to the CIO, bubbles on the Si surface attach at the border and do not lift off until they have enough buoyancy force to overcome the surface force. According to the Fritz model [23], the bubble departure diameter on Si surfaces in water during pool boiling is around 3 mm that is very similar to the bubble size shown in Fig. 6(*a*). Bubble departure diameter by the Fritz model can be evaluated using the equation below:

$$D_b = 0.0208\theta\sqrt{\frac{\sigma}{g(\rho_f - \rho_g)}} \quad (1)$$

Near the heat flux of 80% of CHF, most of the heated area is covered by a large bubble and bubble departing frequency, f_b decreases significantly. With further increase in heat flux, the boiling regime is changed to film boiling, which corresponds to CHF.

Conclusions

This study explores heat transfer characteristics of microporous copper using water. We demonstrate microporous copper inverse opal films by employing templated-electrodeposition technique. Experimental results measuring effective heat transfer coefficient and CHF are obtained during pool boiling tests for a CIO sample with 5 μm pore size. The obtained results are compared to the values of a plain Si surface showing improvements in both HTC and CHF using CIO. We summarize our findings as follows:

(1) The microporous copper inverse opals are fabricated using a copper electrodeposition process around sacrificial polystyrene spheres as a template.
(2) A maximum heat dissipation of $q'' = 225$ W/cm^2 is achieved using the CIO sample with 5 μm pore size. This is almost 3× enhancement in CHF compared to the value of the plain Si.
(3) Effective heat transfer coefficient of the CIO shows a range of 30–117 kW/m^2 K over a range of heat flux of 20–225 W/cm^2, which is 3× improvement compared to the HTC of plain Si.
(4) Bubble departure diameter and frequency are observed from optical images using a high-speed camera. Further studies are required to investigate detailed relationships between pore sizes, contact angles, and bubble departure diameters.

Acknowledgment

The authors are grateful for support of this project by the U.S. Defense Advanced Research Projects Agency Microsystems Technology Office ICECool Fundamentals Program, National Science Foundation sponsored Center for Power Optimization of Electro-Thermal Systems (POETS), and the Institute of Civil Military Technology Cooperation under the Agency for Defense Development (17DB1500).

Nomenclature

D_b = Bubble diameter, m
f_b = bubble departure frequency
g = gravitational acceleration
q'' = heat flux
T = temperature
ΔT_{SH} = wall superheat

Greek Symbols

θ = contact angle
ρ = density
σ = surface tension

Subscripts

CHF = critical heat flux
f = liquid
g = vapor
sat = saturation
SH = superheat
Si = top surface of Si substrate
W = heated surface

References

[1] Bar-Cohen, A., 2013, "Gen-3 Thermal Management Technology: Role of Microchannels and Nanostructures in an Embedded Cooling Paradigm," ASME J. Nanotechnol. Eng. Med., **4**(2), p. 020907.
[2] Won, Y., Cho, J., Agonafer, D., Asheghi, M., and Goodson, K. E., 2013, "Cooling Limits for GaN HEMT Technology," IEEE Compound Semiconductor Integrated Circuit Symposium (CSICS), Monterey, CA, Oct. 13–16, pp. 1–5.
[3] Bar-Cohen, A., and Geisler, K. J. L., 2011, "Cooling the Electronic Brain: Stacking Processing Chips Can Make for More Compact Computers. But it Will Take Advances in Microfluidics to Make Such Dense Number Crunching Practical," Mech. Eng.; New York, **133**(4), pp. 38–41.
[4] Andresen, M., Liserre, M., and Buticchi, G., 2014, "Review of Active Thermal and Lifetime Control Techniques for Power Electronic Modules," 16th European Conference on Power Electronics and Applications (EPE-ECCE), Lappeenranta, Finland, Aug. 26–28, pp. 1–10.
[5] Dhillon, N. S., Buongiorno, J., and Varanasi, K. K., 2015, "Critical Heat Flux Maxima During Boiling Crisis on Textured Surfaces," Nat. Commun., **6**(1), p. 8247.
[6] Chu, K.-H., Enright, R., and Wang, E. N., 2012, "Structured Surfaces for Enhanced Pool Boiling Heat Transfer," Appl. Phys. Lett., **100**(24), p. 241603.
[7] Dullien, F. A. L., 2012, *Porous Media: Fluid Transport and Pore Structure*, Academic Press, Cambridge, MA.
[8] Ohadi, M., Choo, K., Dessiatoun, S., and Cetegen, E., 2013, *Next Generation Microchannel Heat Exchangers*, Springer, New York.
[9] Liu, T., Houshmand, F., Gorle, C., Scholl, S., Lee, H., Won, Y., Asheghi, M., Goodson, K., Kazemi, H., and Vanhille, K., 2015, "Full Scale Simulation of an Integrated Monolithic Heat Sink for Thermal Management of a High Power Density GaN-SiC Chip," ASME Paper No. IPACK2015-48592.
[10] Husain, A., and Kim, K.-Y., 2013, "Design Optimization of Manifold Microchannel Heat Sink Through Evolutionary Algorithm Coupled With Surrogate Model," IEEE Trans. Compon., Packaging Manuf. Technol., **3**(4), pp. 617–624.
[11] McCarthy, M., 2015, "Recent Advancements in Micro/Nanoscale Surface Modifications and Their Effects on Pool Boiling Critical Heat Flux and Heat Transfer Coefficient," *Encyclopedia of Two-Phase Heat Transfer and Flow II*, World Scientific, Singapore, pp. 275–309.
[12] Kaviany, M., 2012, *Principles of Heat Transfer in Porous Media*, Springer Science & Business Media, Berlin.
[13] Chen, R., Lu, M.-C., Srinivasan, V., Wang, Z., Cho, H. H., and Majumdar, A., 2009, "Nanowires for Enhanced Boiling Heat Transfer," Nano Lett., **9**(2), pp. 548–553.
[14] Mori, S., Mt Aznam, S., and Okuyama, K., 2015, "Enhancement of the Critical Heat Flux in Saturated Pool Boiling of Water by Nanoparticle-Coating and a Honeycomb Porous Plate," Int. J. Heat Mass Transfer, **80**, pp. 1–6.
[15] Jaikumar, A., and Kandlikar, S. G., 2016, "Pool Boiling Enhancement Through Bubble Induced Convective Liquid Flow in Feeder Microchannels," Appl. Phys. Lett., **108**(4), p. 041604.
[16] Palko, J. W., Lee, H., Zhang, C., Dusseault, T. J., Maitra, T., Won, Y., Agonafer, D. D., Moss, J., Houshmand, F., Rong, G., Wilbur, J. D., Rockosi, D., Mykyta, I., Resler, D., Altman, D., Asheghi, M., Santiago, J. G., and Goodson, K. E., 2017, "Extreme Two-Phase Cooling From Laser-Etched Diamond and Conformal, Template-Fabricated Microporous Copper," Adv. Funct. Mater., **27**(45), p. 1703265.
[17] Palko, J. W., Zhang, C., Wilbur, J. D., Dusseault, T. J., Asheghi, M., Goodson, K. E., and Santiago, J. G., 2015, "Approaching the Limits of Two-Phase Boiling Heat Transfer: High Heat Flux and Low Superheat," Appl. Phys. Lett., **107**(25), p. 253903.
[18] Barako, M. T., Sood, A., Zhang, C., Wang, J., Kodama, T., Asheghi, M., Zheng, X., Braun, P. V., and Goodson, K. E., 2016, "Quasi-Ballistic Electronic Thermal Conduction in Metal Inverse Opals," Nano Lett., **16**(4), pp. 2754–2761.
[19] Bigioni, T. P., Lin, X.-M., Nguyen, T. T., Corwin, E. I., Witten, T. A., and Jaeger, H. M., 2006, "Kinetically Driven Self Assembly of Highly Ordered Nanoparticle Monolayers," Nat. Mater., **5**(4), pp. 265–270.
[20] Barako, M. T., Roy-Panzer, S., English, T. S., Kodama, T., Asheghi, M., Kenny, T. W., and Goodson, K. E., 2015, "Thermal Conduction in Vertically

Aligned Copper Nanowire Arrays and Composites," ACS Appl. Mater. Interfaces, **7**(34), pp. 19251–19259.
[21] Anderson, T. M., and Mudawar, I., 1989, "Microelectronic Cooling by Enhanced Pool Boiling of a Dielectric Fluorocarbon Liquid," ASME J. Heat Transfer, **111**(3), pp. 752–759.
[22] Ujereh, S., Fisher, T., and Mudawar, I., 2007, "Effects of Carbon Nanotube Arrays on Nucleate Pool Boiling," Int. J. Heat Mass Transfer, **50**(19–20), pp. 4023–4038.
[23] Kocamustafaogullari, G., and Ishii, M., 1983, "Interfacial Area and Nucleation Site Density in Boiling Systems," Int. J. Heat Mass Transfer, **26**(9), pp. 1377–1387.